**Statistical analysis.** Statistical differences were determined using one-way ANOVA followed by post-hoc comparison with the Fisher's protected least significant difference test. Statistical significance is displayed as $P < 0.05$ (one asterisk) or $P < 0.01$ (two asterisks).

*Note: Supplementary Information is available on the Nature Cell Biology website.*


## ACKNOWLEDGEMENTS

We thank T. Watanabe, H. Shiina, J. Miyamoto, K. Sekine, R. Fujiki, Y. Imai and S. Tanaka for generation of knockout mice, and H. Higuchi for manuscript preparation. This work was supported in part by the Program for Promotion of Basic Research Activities for Innovative Biosciences (PROBRAIN) and priority areas from the Ministry of Education, Culture, Sports, Science and Technology (to S.K.).


## AUTHOR CONTRIBUTIONS

The experimental concept was developed by S.K., B.W.O.M, S.T., K.T., H.E. and H.K. T.F., K.Y. and S.F. conducted most of experiments, and I.K., K.Y., M.M., M.N., T.N., C.A., Y.Y., T.K., C.F. and S.T. contributed materials and supported several experiments. S.K., T.F., K.Y. and S.F. wrote the manuscript.

## COMPETING FINANCIAL INTERESTS

The authors declare that they have no competing financial interests.


Published online at http://www.nature.com/naturecellbiology/
Reprints and permissions information is available online at http://npg.nature.com/reprintsandpermissions/



1. Carthew, R. W. Gene regulation by microRNAs. *Curr. Opin. Genet. Dev.* **16,** 203–208 (2006).
2. Cullen, B. R. Transcription and processing of human microRNA precursors. *Mol. Cell* **16,** 861–865 (2004).
3. Filipowicz, W., Jaskiewicz, L., Kolb, F. A. & Pillai, R. S. Post-transcriptional gene silencing by siRNAs and miRNAs. *Curr. Opin. Struct. Biol.* **15,** 331–341 (2005).
4. Kim, V. N. MicroRNA biogenesis: coordinated cropping and dicing. *Nature Rev. Mol. Cell Biol.* **6,** 376–385 (2005).
5. Valencia-Sanchez, M. A., Liu, J., Hannon, G. J. & Parker, R. Control of translation and mRNA degradation by miRNAs and siRNAs. *Genes Dev.* **20,** 515–524 (2006).
6. Zamore, P. D. & Haley, B. Ribo-gnome: the big world of small RNAs. *Science* **309,** 1519–1524 (2005).
7. Gregory, R. I. *et al.* The Microprocessor complex mediates the genesis of microRNAs. *Nature* **432,** 235–240 (2004).
8. Hirling, H., Scheffner, M., Restle, T. & Stahl, H. RNA helicase activity associated with the human p68 protein. *Nature* **339,** 562–564 (1989).
9. Huang, Y. & Liu, Z. R. The ATPase, RNA unwinding, and RNA binding activities of recombinant p68 RNA helicase. *J. Biol. Chem.* **277,** 12810–12815 (2002).
10. Lamm, G. M., Nicol, S. M., Fuller-Pace, F. V. & Lamond, A. I. p72: a human nuclear DEAD box protein highly related to p68. *Nucleic Acids Res.* **24,** 3739–3747 (1996).
11. Auboeuf, D., Honig, A., Berget, S. M. & O'Malley, B. W. Coordinate regulation of transcription and splicing by steroid receptor coregulators. *Science* **298,** 416–419 (2002).
12. Bates, G. J. *et al.* The DEAD box protein p68: a novel transcriptional coactivator of the p53 tumour suppressor. *EMBO J.* **24,** 543–553 (2005).
13. Causevic, M. *et al.* Overexpression and poly-ubiquitylation of the DEAD-box RNA helicase p68 in colorectal tumours. *Oncogene* **20,** 7734–7743 (2001).
14. Dubey, P. *et al.* The immunodominant antigen of an ultraviolet-induced regressor tumor is generated by a somatic point mutation in the DEAD box helicase p68. *J. Exp. Med.* **185,** 695–705 (1997).
15. Endoh, H. *et al.* Purification and identification of p68 RNA helicase acting as a transcriptional coactivator specific for the activation function 1 of human estrogen receptor alpha. *Mol. Cell Biol.* **19,** 5363–5372 (1999).
16. Kircher, S. G., Kim, S. H., Fountoulakis, M. & Lubec, G. Reduced levels of DEAD-box proteins DBP-RB and p72 in fetal Down syndrome brains. *Neurochem. Res.* **27,** 1141–1146 (2002).
17. Watanabe, M. *et al.* A subfamily of RNA-binding DEAD-box proteins acts as an estrogen receptor alpha coactivator through the N-terminal activation domain (AF-1) with an RNA coactivator, SRA. *EMBO J.* **20,** 1341–1352 (2001).
18. Boehm, M. & Slack, F. A developmental timing microRNA and its target regulate life span in *C. elegans*. *Science* **310,** 1954–1957 (2005).
19. Yang, W. J. *et al.* Dicer is required for embryonic angiogenesis during mouse development. *J. Biol. Chem.* **280,** 9330–9335 (2005).
20. Lee, Y. *et al.* The nuclear RNase III Drosha initiates microRNA processing. *Nature* **425,** 415–419 (2003).
21. Wu, H., Xu, H., Miraglia, L. J. & Crooke, S. T. Human RNase III is a 160-kDa protein involved in preribosomal RNA processing. *J. Biol. Chem.* **275,** 36957–36965 (2000).
22. Han, J. *et al.* The Drosha–DGCR8 complex in primary microRNA processing. *Genes Dev.* **18,** 3016–3027 (2004).
23. Ni, J. Q., Liu, L. P., Hess, D., Rietdorf, J. & Sun, F. L. *Drosophila* ribosomal proteins are associated with linker histone H1 and suppress gene transcription. *Genes Dev.* **20,** 1959–1973 (2006).
24. Kitagawa, H. *et al.* The chromatin-remodeling complex WINAC targets a nuclear receptor to promoters and is impaired in Williams syndrome. *Cell* **113,** 905–917 (2003).
25. Yanagisawa, J. *et al.* Nuclear receptor function requires a TFTC-type histone acetyl transferase complex. *Mol. Cell* **9,** 553–562 (2002).
26. Denli, A. M., Tops, B. B., Plasterk, R. H., Ketting, R. F. & Hannon, G. J. Processing of primary microRNAs by the Microprocessor complex. *Nature* **432,** 231–235 (2004).
27. Ogilvie, V. C. *et al.* The highly related DEAD box RNA helicases p68 and p72 exist as heterodimers in cells. *Nucleic Acids Res.* **31,** 1470–1480 (2003).
28. Bernstein, E. *et al.* Dicer is essential for mouse development. *Nature Genet.* **35,** 215–217 (2003).
29. Lu, J. *et al.* MicroRNA expression profiles classify human cancers. *Nature* **435,** 834–838 (2005).
30. Otte, A. P. & Kwaks, T. H. Gene repression by Polycomb group protein complexes: a distinct complex for every occasion? *Curr. Opin. Genet. Dev.* **13,** 448–454 (2003).
31. Perissi, V. & Rosenfeld, M. G. Controlling nuclear receptors: the circular logic of cofactor cycles. *Nature Rev. Mol. Cell Biol.* **6,** 542–554 (2005).
32. Iggo, R. D. & Lane, D. P. Nuclear protein p68 is an RNA-dependent ATPase. *EMBO J.* **8,** 1827–1831 (1989).
33. Han, J. *et al.* Molecular basis for the recognition of primary microRNAs by the Drosha–DGCR8 complex. *Cell* **125,** 887–901 (2006).
34. Fujiki, R. *et al.* Ligand-induced transrepression by VDR through association of WSTF with acetylated histones. *EMBO J* **24,** 3881–3894 (2005).
35. Ohtake, F. *et al.* Modulation of oestrogen receptor signalling by association with the activated dioxin receptor. *Nature* **423,** 545–550 (2003).

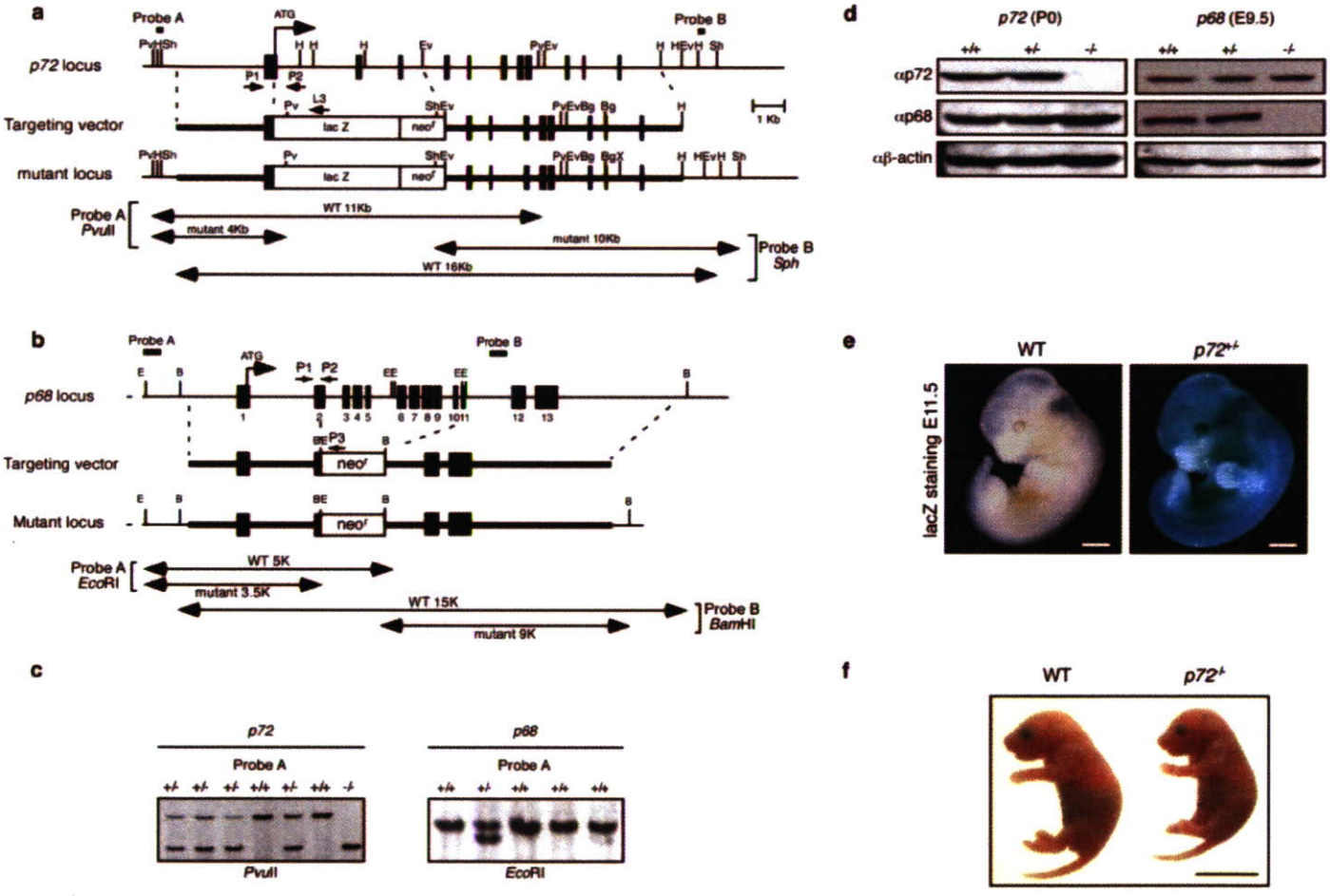


**Figure S1** Targeted disruption of the *p68* and *p72* genes. **(a)** Scheme of the genomic structure of *p72* locus (top), targeting vector (middle) and predicted mutant locus (bottom). Southern blot probes and PCR primers (P1, P2 and L3) used for genotyping are indicated. Southern blot fragments detected by each probe are indicated by arrows. Restriction sites indicated are *Pvu*II (Pv), *Hind*III (H), *Sph*I (Sh), and *Eco*RV (Ev). **(b)** Scheme of the genomic structure of *p68* locus (top), targeting vector (middle) and predicted mutant locus (bottom). Filled boxes indicate exons. Southern blot probes (probe A, B) and PCR primers (P1, P2 and P3) used for genotyping are indicated. Southern blot fragments detected by each probe are indicated by arrows. Restriction sites indicated are *Eco*RI (E) and *Bam*HI (B). **(c)** Southern blot analysis of the offspring obtained by heterozygous cross. Genomic DNA from *p72* F2 tails was digested with *Pvu*II and detected by Probe A as described S1a (left). Genomic DNAs from *p68* F2 yolk sacs were digested with *Eco*RI and detected by Probe A as described S1b (right). **(d)** Both $p68^{-/-}$ and $p72^{-/-}$ mice were null in protein expression. Western blot analysis of p72 protein in P0 liver (left) and p68 protein in E9.5 embryos (right) of the indicated genotype. **(e)** Expression of lacZ driven by the p72 endogenous promoter. E11.5 embryo was visualized by whole-mount lacZ staining. The scale bars represent 1 mm. **(f)** Body size of $p72^{-/-}$ pups and WT littermates (P2). The scale bars represent 10 mm.

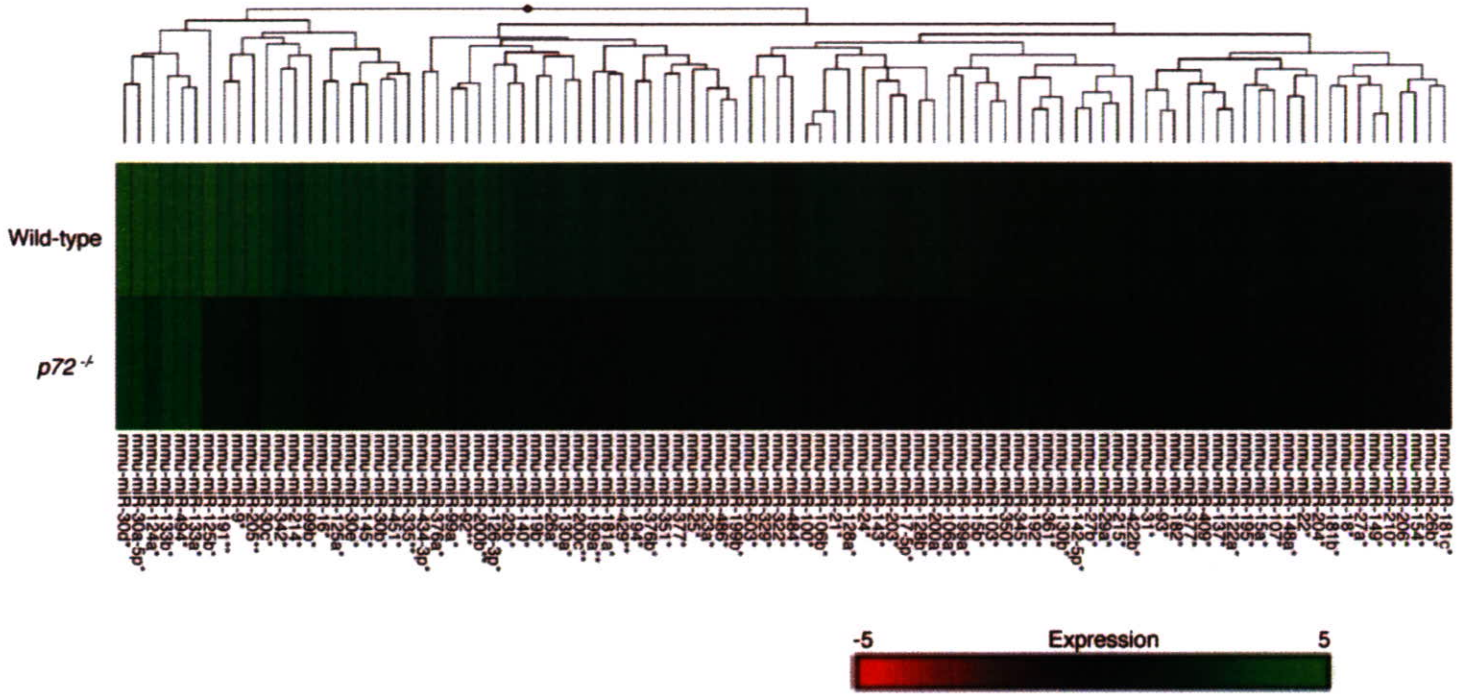


**Figure S2** Microarray expression profile of 266 mouse miRNAs in *p72*$^{-/-}$ embryos (E18.5) compared with WT embryos (n=3 per genotype). Relative expression levels for the 94 miRNAs that changed significantly and more than 1.5 fold in three experiments are shown (*$p < 0.05$; **$p < 0.01$ with one-way ANOVA).

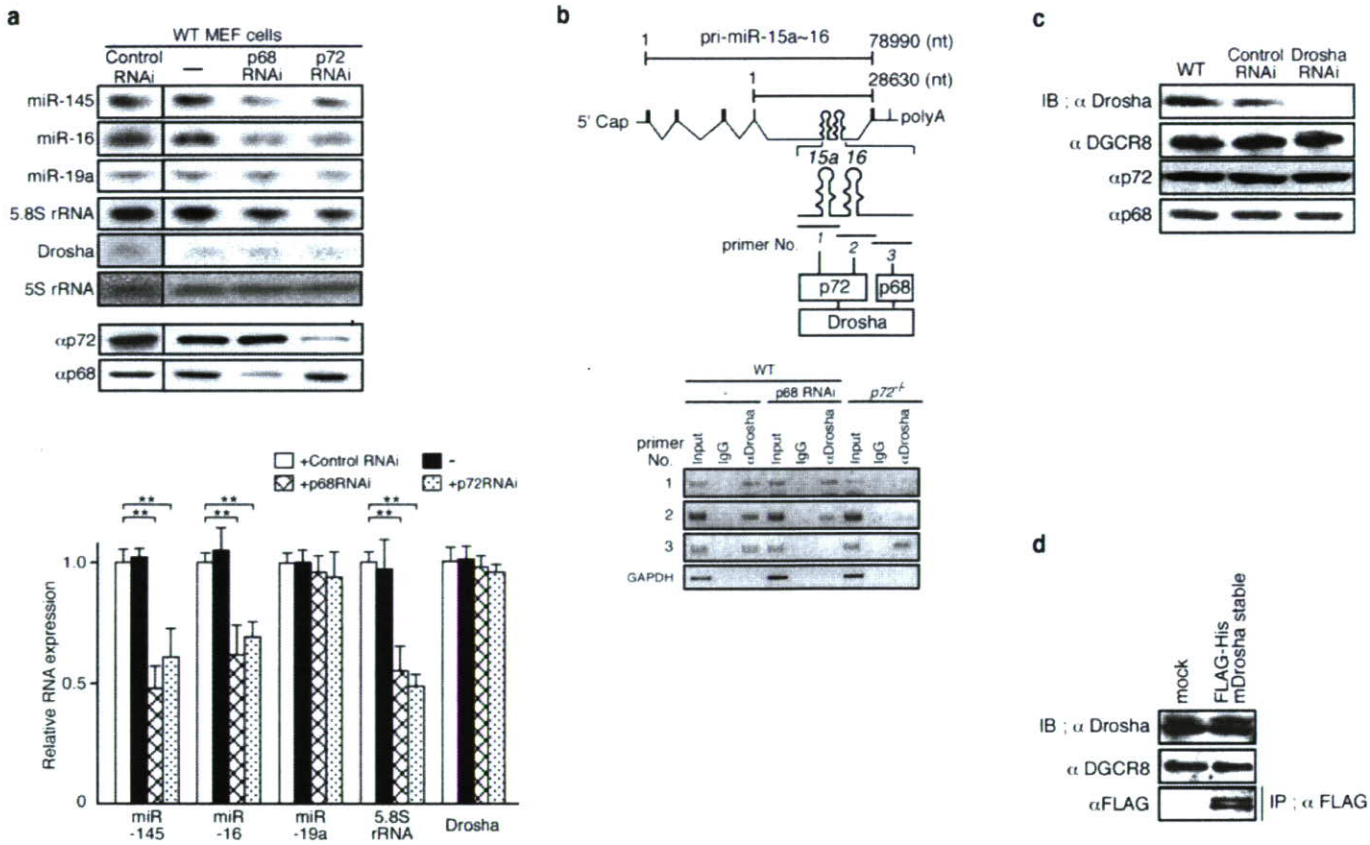


**Figure S3 (a)** Northern blot analysis of miRNAs and 5.8S rRNA of WT MEF cells transfected with control RNAi, p68 RNAi or p72 RNAi. Results are expressed as the mean ±SD of four independent experiments. Lower bar graph indicates the results from upper panel Northern blots, expressed as the mean ± SD of four independent experiments. Significant differences when compared with the data for WT MEF cells with control RNAi are shown (**p <0.01 with one-way ANOVA). **(b)** RNA-ChIP analysis was performed to estimate the p68, p72 and Drosha binding sites on pri-miR-15a and pri-miR-16. Schematic representation of the hairpin structure between pri-miR-15a and pri-miR-16 (upper). Ethidium bromide stained agarose gels of each RT-PCR products (lower). The numbers under the pri-miRNAs indicate the positions of primer pairs used for RNA-ChIP analysis. Indicated p68, p72 and Drosha binding sites in pri-miR-15a and pri-miR-16 were deduced from results shown lower panels. ChIP samples were prepared from WT MEF cells transfected with p68 RNAi or without, and *p72*$^{-/-}$ MEF cells. RT-PCR was carried out on total-input RNA and RNA precipitated with IgG (negative control) or anti-Drosha antibody. **(c)** Efficiency of Drosha knockdown by RNAi. WT MEF cells were transfected with or without indicated siRNA. Expression levels of Drosha, DGCR8, p72 and p68 were examined by Western blotting. **(d)** Comparison of mDrosha expression in the mock and FLAG-His-mDrosha stable transfected MCT cells. The expression levels of mDrosha and DGCR8 proteins were estimated by Western blotting.

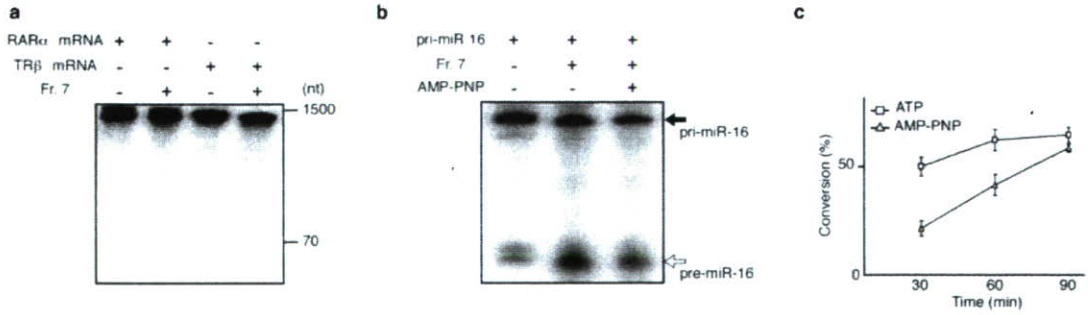


**Figure S4** Selective and ATP-dependent processing of RNA processing by the purified mDrosha complex. **(a)** No cleavage of mRNAs by the purified mDrosha complex. *In vitro* transcribed mRNAs of human RARα and TRβ were applied for the *in vitro* processing assay by the purified complex, and no clear cleavage was detected. **(b)** ATP-dependent processing of pre-miRNA by the purified complex. The *in vitro* processing of pri-miR-16 was attenuated in the presence of an ATP analog, AMP-PNP; Adenosine 5'-triphosphate tetralithium salt hydrate (1 mM). **(c)** Time-course analysis of the ATP analog effect on pre-miRNA processing. Pri-miR-16 was incubated with 10 mM ATP (square) or 10 mM AMP-PNP (triangle) for indicated times.

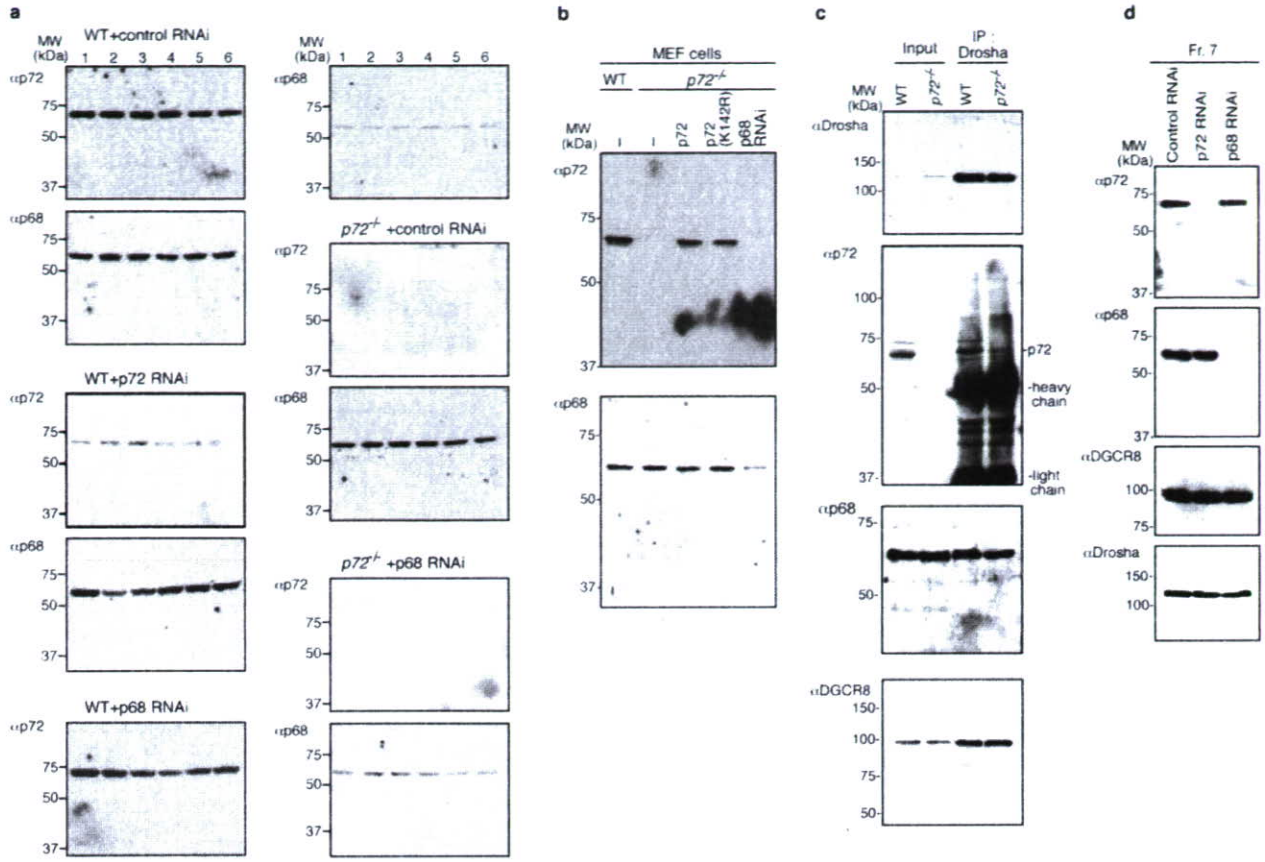


**Figure S5** Selected representative full-scan images. For a, c, and d, full sized membranes were cut prior to immunoblotting according to prestained MW markers. **(a)** Images correspond to Fig. 1e. **(b)** Images correspond to Fig. 2c. **(c)** Images correspond to Fig. 4a. **(d)** Images correspond to Fig. 5f.

**References**


1. Sato, T. *et al.* Brain masculinization requires androgen receptor function. *Proc Natl Acad Sci U S A* **101**, 1673-8 (2004).
2. Sekine, K. *et al.* Fgf10 is essential for limb and lung formation. *Nat Genet* **21**, 138-41 (1999).
3. Shiina, H. *et al.* Premature ovarian failure in androgen receptor-deficient mice. *Proc Natl Acad Sci U S A* **103**, 224-9 (2006).
4. Kitagawa, H. *et al.* The chromatin-remodeling complex WINAC targets a nuclear receptor to promoters and is impaired in Williams syndrome. *Cell* **113**, 905-17 (2003).
5. Taganov, K.D., Boldin, M.P., Chang, K.J. & Baltimore, D. NF-kappaB-dependent induction of microRNA miR-146, an inhibitor targeted to signaling proteins of innate immune responses. *Proc Natl Acad Sci U S A* **103**, 12481-6 (2006).
6. Morgenstern, B. DIALIGN 2: improvement of the segment-to-segment approach to multiple sequence alignment. *Bioinformatics* **15**, 211-8 (1999).
7. Morgenstern, B., Frech, K., Dress, A. & Werner, T. DIALIGN: finding local similarities by multiple sequence alignment. *Bioinformatics* **14**, 290-4 (1998).

**Supplementary Information**

## Materials and Methods

### Material

For RNA ChIP primers;

pri-miR-16 (each primer number is referred for supplementary figure 3b)

1 ; Forward primer 5'-TGCTATCATAGGAGCTATGAATAAAAA-3'

Reverse primer 5'-CTTTTTCCTAAAAAGCCTTTTCTGTAAATT-3'

2 ; Forward primer 5'-AGAAAAACCGTGTAAACACACAAGT-3'

Reverse primer 5'-CAAGGACCTGATCTTCTGAAGAGAG-3'

3 ; Forward primer 5'-CATGCTAGCAAGAAGCACTTGGCCA-3'

Reverse primer 5'-TACTCTACAACTGTAATTCAATGTGTA-3'

pri-miR-214 (each primer number is referred for Figure 3)

1 ; Forward primer 5'-CGGTGTGTGGAAAATCCTGTCCCGG-3'

Reverse primer 5'-TGCCCAGTTGAGGGAAAAAATCTGG-3'

2 ; Forward primer 5'-TTGGAAGCAGCACATTGTGTCCCCA-3'

Reverse primer 5'-AGTCGATGCAGCAGACAGGGTTCAG-3'

3 ; Forward primer 5'-AGTTTAAGTCTCTGAATTATCAGTT-3'

Reverse primer 5'-AACGCCATGGACGGCTGGGGACACA-3'

4 ; Forward primer 5'-ACAACGTGCCTTATCATTTCAAAGG-3'

Reverse primer 5'-ATAATTCAGAGACTTAAACTCGAGC-3'

5 ; Forward primer 5'-TCAGAGATGCAGCTATACTATAGTA-3'

Reverse primer 5'-GAAATGATAAGGCACGTTGTCTAAA-3'

6 ; Forward primer 5'-CTGTGAAGAAAGGTTATTCTTCTTG-3'

Reverse primer 5'-AAAGGAGAGTGCAAACTCTCCTTAG-3'

7 ; Forward primer 5'-GACTTACCATACTATCCAGAGCAAG-3'

Reverse primer 5'-CAAGAAGAATAACCTTTCTTCACAG-3'

8 ; Forward primer 5'-AAATACTTGGGTGGTCCATAGGCAA-3'

Reverse primer 5'-GGGCAGAAGAGAGTAACCAGCAGCA-3'

9 ; Forward primer 5'-ATGATTTTCTTTAACTCAGATGACT-3'

Reverse primer 5'-TATGGACCACCCAAGTATTTCACTC-3'

10 ; Forward primer 5'-ATCTAAAATGTTTGAGGCTAAACTA-3'

Reverse primer 5'-TCTGAGTTAAAGAAAATCATCAAGT-3'

11 ; Forward primer 5'-GAACAATAAAATCTTTTTTGAGAAT-3'

Reverse primer 5'-TAGCCTCAAACATTTTAGATAGCAT-3'

12 ; Forward primer 5'-GCTTCTATCCCCCTTGATTAACAAG-3'

Reverse primer 5'-TTTATTGTTCATAAAACTTCTGCCT-3'

13 ; Forward primer 5'-AAAAAGAAGTTAGACGTTTGGCTTT-3'

Reverse primer 5'-TAATCAAGGGGGATAGAAGCTTATG-3'

14 ; Forward primer 5'-CTTGGGTCCTTCAGGTTTCCTTTGC-3'

Reverse primer 5'-CAAACGTCTAACTTCTTTTTAGTTC-3'

15 ; Forward primer 5'-CAGCTTTCTTTCAATGGCTGGTGGT-3'

Reverse primer 5'-CTGATTGTATCTGTCCCTGAGCAAA-3'

16 ; Forward primer 5'-TTACCCAGGCCAGACTGGCAGTTTG-3'

Reverse primer 5'-ACCACCAGCCATTGAAAGAAAGCTG-3'

17 ; Forward primer 5'-TTTTCTAAATTTACCTGTCTCTGCA-3'

Reverse primer 5'-CAATATATTCTAAAGGATCAAGTAT-3'

18 ; Forward primer 5'-TGATGTATCATTCAGCATTCTGTTG-3'

Reverse primer 5'-AGACAGGTAAATTTAGAAAATTATT-3'

19 ; Forward primer 5'-AATACACGGTAATGGCCAGTGCCAT-3'

Reverse primer 5'-GAATGCTGAATGATACATCACAAAA-3'

20 ; Forward primer 5'-TGCCTTCTCACGTAGCCCTTTCTAA-3'

Reverse primer 5'-ACTGGCCATTACCGTGTATTAAATA-3'

**Construction of *p68* and *p72* targeting vectors**

A 2.8-kb upstream and a 7.5-kb downstream region of *p72* genomic fragment were obtained from RPCI.23-146P10 BAC clone, to generate the targeting vector with lacZ and PGK-neo cassette to replace the translation initiation site. A 3.0-kb 5' and a 7.1-kb 3' homologous region of *p68* genomic fragment were obtained from RPCI.23-247J12 BAC clone for the targeting vector.

**Generation of *p68*, and *p72* knockout mice**

TT2 ES cells were electroporated with the linearized targeting vector and selected by G418. Two (p72) and three (p68) independent ES clones were isolated as homologous

recombinants by Southern blot analysis [1-3]. These ES clones were aggregated with single eight-cell embryo from CD-1 mice. Germline chimeras were bred to C57BL/6J female mice to generate heterozygous mutant F1 mice. For genotyping, high-molecular weight genomic DNA isolated from mouse tails or yolk sacs was subjected to either Southern blot analysis or PCR analysis with 5'-3' probes.

**Whole-mount lacZ staining**

For lacZ staining, embryos were fixed in PBS containing 1% formaldehyde, 0.2% glutaraldehyde, and 0.02% NP-40 [4]. After fixation, embryos were placed in staining buffer [44 mM HEPES (pH 7.4), 3 mM potassium ferricyanide, 15 mM NaCl, 1.3 mM $MgCl_2$, 0.5 mg/ml 5-bromo-4-chloro-3-indolyl-b-galactopyranoside (X-gal)] at room temperature.

**MicroRNA microarray**

Microarray experimental procedures were performed as previously described [5]. Briefly, total RNA was isolated from whole E18.5 embryos by using the *mir*Vana™ RNA Isolation kit (Ambion, Austin, TX) according to the manufacture's protocol. A flashPAGE™ fractionator System (Ambion) was used to isolate miRNA from total RNA. One hundred micrograms of total RNA was enriched for small RNA species, tailed by using the *mir*Vana™ miRNA Labeling Kit (Ambion), and fluorescently labeled by using the CyDye Mono-Reactive Dye Pack (GE Healthcare Bio-Science Corp., Piscataway, NJ, USA). Unincorporated dyes were removed with a second glass

fiber filter-based cleaning procedure. Hybridization was carried out on DNA oligonucleotide probes from the *mir*Vana$^{TM}$ miRNA Bioarray V2 (Ambion) containing 266 mouse miRNAs in four copies. Following hybridization, the miRNA arrays were scanned using a GenePix 4000B scanner (Axon Instruments, CA, USA). Raw data were normalized and analyzed using Array-Pro Analyzer Version 4.5 (Media Cybernetics, Inc., Silver Spring, MD, USA). Analyzed data were selected by using MicroArray Data Analysis Tool (Filgen, Inc.). Cluster analysis [6,7] was performed using Spotfire DecisionSite Functional Genomics (Spotfire Inc. Somerville, MA), applying clustering methods: Complete linkage (maximum), similarity measure: Euclidean distance and ordering Average value. Differentially expressed miRNAs were identified using one-way ANOVA followed by post hoc comparison with the Fisher's protected least significant difference test.

**Whole-mount *in situ* hybridization, histology, and immunohistochemistry**

Whole-mount *in situ* hybridization using digoxigenin-labelled probes was performed as previously described [4]. Each *p68* and *p72* cDNA was used as a template for riboprobe synthesis. For histological analysis, embryos and tissues were fixed with 4% paraformaldehyde in PBS and embedded in paraffin. The sections were deparaffinized, rehydrated, and stained with thionine, hematoxylin and eosin. Immunohistochemistry was performed as previously described [4].

**Western blot analysis**

For Western blot analysis, whole embryos and cell lysates were prepared in TNE buffer [10 mM Tris-HCl (pH 7.5), 1% NP-40, 0.15 M NaCl, 1 mM EDTA]. Proteins were separated by SDS-PAGE and Western blotted using standard conditions [4].

**Immunoprecipitation**

For immunoprecipitation, cells were lysed in TNE buffer. Extract from wild-type or *p72*$^{-/-}$ MEF cells were immunoprecipitated with anti-Drosha antibody and protein G sepharose. After washing, the immunoprecipitates were subjected to Western blotting analysis [4].

nature cell biology

# A histone lysine methyltransferase activated by non-canonical Wnt signalling suppresses PPAR-γ transactivation

Ichiro Takada[1], Masatomo Mihara[1,3], Miyuki Suzawa[1], Fumiaki Ohtake[1,2], Shinji Kobayashi[1,2], Mamoru Igarashi[1], Min-Young Youn[1], Ken-ichi Takeyama[1], Takashi Nakamura[1,2], Yoshihiro Mezaki[1], Shinichiro Takezawa[1], Yoshiko Yogiashi[1], Hirochika Kitagawa[1], Gen Yamada[4], Shinji Takada[5], Yasuhiro Minami[6], Hiroshi Shibuya[7], Kunihiro Matsumoto[8] and Shigeaki Kato[1,2,9]

**Histone modifications induced by activated signalling cascades are crucial to cell-lineage decisions. Osteoblast and adipocyte differentiation from common mesenchymal stem cells is under transcriptional control by numerous factors. Although PPAR-γ (peroxisome proliferator activated receptor-γ) has been established as a prime inducer of adipogenesis, cellular signalling factors that determine cell lineage in bone marrow remain generally unknown. Here, we show that the non-canonical Wnt pathway through CaMKII–TAK1–TAB2–NLK transcriptionally represses PPAR-γ transactivation and induces Runx2 expression, promoting osteoblastogenesis in preference to adipogenesis in bone marrow mesenchymal progenitors. Wnt-5a activates NLK (Nemo-like kinase), which in turn phosphorylates a histone methyltransferase, SETDB1 (SET domain bifurcated 1), leading to the formation of a co-repressor complex that inactivates PPAR-γ function through histone H3-K9 methylation. These findings suggest that the non-canonical Wnt signalling pathway suppresses PPAR-γ function through chromatin inactivation triggered by recruitment of a repressing histone methyltransferase, thus leading to an osteoblastic cell lineage from mesenchymal stem cells.**

Histone modification on chromatin regulates transcription. Several post-translational and covalent modifications of histones have been documented, for example, methylation of lysine and arginine residues, acetylation of lysine, phosphorylation of serine and threonine residues and sumoylation of lysine. Accumulating evidence has established that hyperacetylation of histone in specific chromosomal regions generally results in activation of a given chromatin area in gene regulation, whereas hypoacetylated histones are indicators of inactive chromatin[1–3]. Other histone modifications are less predictable in how they activate chromatin; however, specific combinations of several histone modifications at certain histone residues are considered to constitute a 'histone code' that defines chromatin states for transcriptional control[1]. Among such histone modifications, lysine methylation results in unique transcriptional outcomes depending on the methylation sites, which act as docking signals for recruiting chromatin remodellers and modifiers[2–4]. Among methylated sites on mammalian chromatin, methylated H3-K9, H3-K27 and H4-K20 are considered as hallmarks of a condensed chromatin state[2]. Furthermore, H3-K9 methylation by histone lysine methyltransferase (HKMTs) triggers heterochromatin formation and transcriptionally silences euchromatic regions by recruiting heterochromatin proteins[3,4]. Reflecting the crucial roles of methylated lysines at specific sites, multiple HKMTs have been identified that recognize the same lysine residue for mono-, di- and/or tri-methylations, although the biological role of each HKMT remains elusive[4,5]. Histone modifications are altered during cell-lineage decisions, and rearrangements of histone modifications take place in response to changes in the extracellular environment[6]. However, the molecular mechanisms underlying these processes remain poorly understood.

Certain nuclear receptors (NRs) have been well researched and have been shown to integrate their ligand signals into the histone code through histone acetylation or deacetylation[7,8]. In the absence of cognate ligands, NRs are transcriptionally silent, associating with

[1]Institute of Molecular and Cellular Biosciences, University of Tokyo, Yayoi 1-1-1, Bunkyo-ku, Tokyo 113-0032, Japan. [2]ERATO, Japan Science and Technology, Honcho 4-1-8, Kawaguchi, Saitama 332-0012, Japan. [3]Department of Medicine and Bioregulatory Sciences, Institute of Health Biosciences, University of Tokushima Graduate School, Kuramoto-3, Tokushima, 770-8503, Japan. [4]Center for Animal Resources and Development (CARD), Graduate School of Medical and Pharmaceutical Sciences, Kumamoto University, Honjo 2-2-1, Kumamoto 860-0811, Japan. [5]Okazaki Institute for Integrative Bioscience, National Institutes of Natural Sciences, Okazaki, Aichi 444-8787, Japan. [6]Department of Genome Sciences, Graduate School of Medicine, Kobe University, Kobe 650-0017, Japan. [7]Department of Molecular Cell Biology, Medical Research Institute and School of Biomedical Science, Tokyo Medical and Dental University, and CREST, JST, Kanda-Surugadai, Chiyoda-ku, Tokyo 101-0062, Japan. [8]Department of Molecular Biology, Graduate School of Science, Nagoya University, Chikusa-ku, Nagoya 464-8602, Japan. [9]Correspondence should be addressed to S.K. (uskato@mail.ecc.u-tokyo.ac.jp)

Received 20 June 2007; accepted 14 September 2007; published online 21 October 2007; DOI: 10.1038/ncb1647

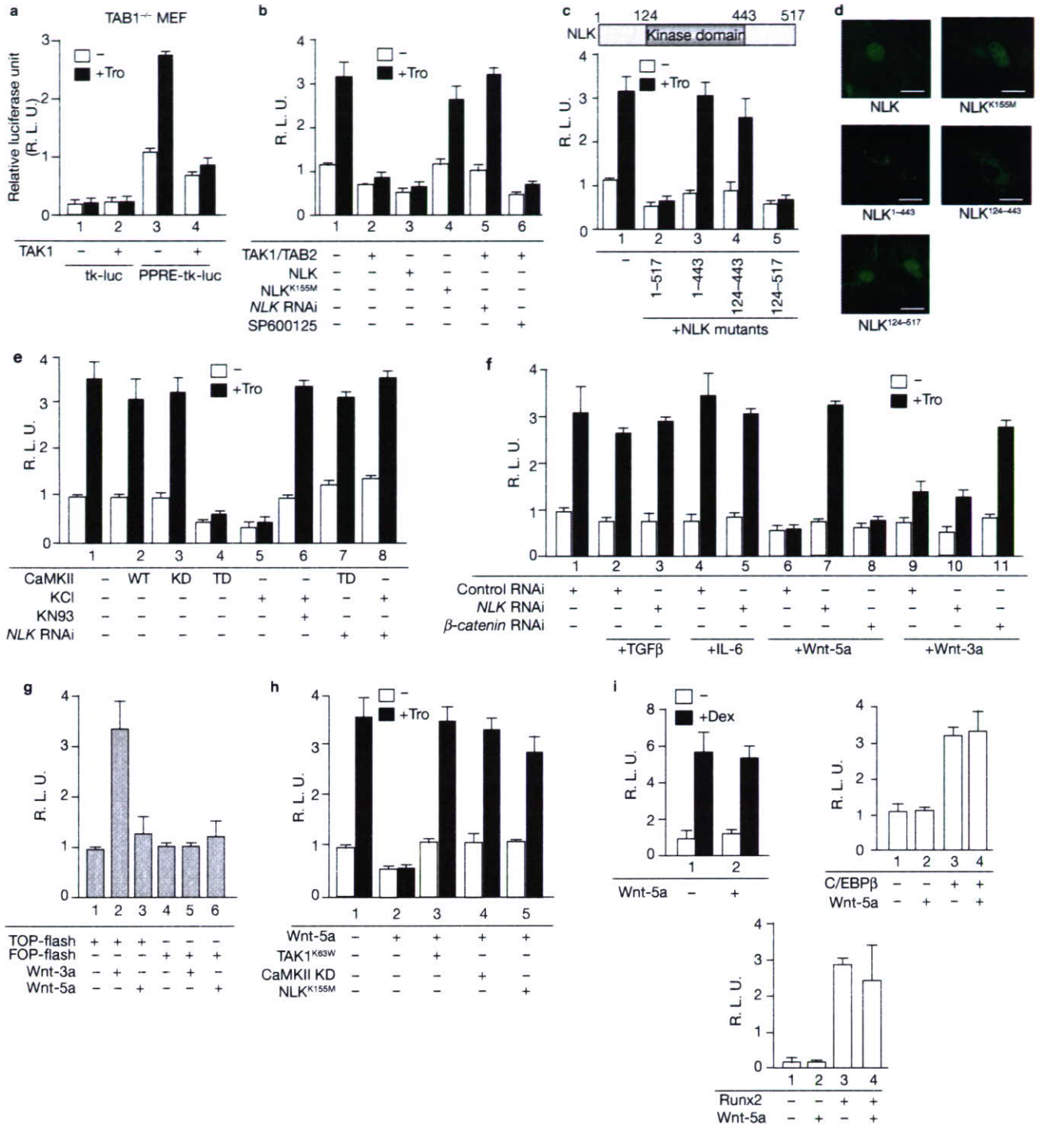


**Figure 1** Wnt-5a signalling suppresses the transactivation function of PPAR-γ through CaMKII–TAK1–TAB2–NLK. (**a**) Luciferase assays in TAB1$^{-/-}$ MEF cells. After transfection with PPAR-γ, TAK1 expression vectors and acyl-CoA-PPRE-tk or tk luciferase vectors (tk-luc, thymidine-kinase-promoter–luciferase), cells were incubated with or without troglitazone (Tro). (**b**) Luciferase assays in ST2 cells transfected with PPRE-tk-luc vector and indicated expression vectors (TAK1, TAB2, PPAR-γ, NLK wild-type and kinase-negative mutants NLK$^{K155M}$), *NLK* RNAi or JNK inhibitor (SP600125). (**c**) Luciferase assays in ST2 cells transfected with PPRE-tk-luc vector and expression vectors of PPAR-γ and NLK deletion mutants. (**d**) ST2 cells transfected with expression vectors of GFP-fusion NLKs were scanned using a Zeiss confocal laser scanning system 510. Scale bars, 50 μm. (**e**) Luciferase assays in ST2 cells transfected with PPRE-tk-luc vector and expression vectors of PPAR-γ, CaMKII or *NLK* RNAi. WT; wild type, TD; active form, KD; kinase-dead form. Luciferase assay in ST2 cells incubated with 50 mM KCl or CaMKII inhibitor (KN93) were also performed (lane 5, 6). (**f**) Luciferase assay in ST2 cells with or without TGF-β, IL-6, Wnt-5a and Wnt-3a. *NLK* or *β-catenin* RNAi was also transfected (lane 3, 5, 7, 8, 10, 11). (**g**) Luciferase assays in ST2 cells transfected with TOP-flash or FOP-flash luc vector (TOP-flash: luc vector containing wild-type β-catenin–TCF-binding site; FOP-flash: luc vector containing mutated β-catenin–TCF-binding site) and incubated with or without Wnt-3a or Wnt-5a. (**h**) Luciferase assays in ST2 cells transfected with PPRE-tk-luc vector and PPRE-γ expression vector with or without Tro, Wnt-5a and indicated expression vectors. (**i**) Luciferase assays in ST2 cells transfected with GR (GR expression vector and GRE-luc), C/EBPβ (C/EBPβ expression vector and C/EBP-RE-tk-luc) or Runx2 (Runx2 expression vector and Runx2-RE-tk-luc). Dexamethasone (100 nM) was used to induce glucocorticoid receptor function. All error bars represent the means±s.d. of triplicate determinations ($n$=5×10$^4$ cells).

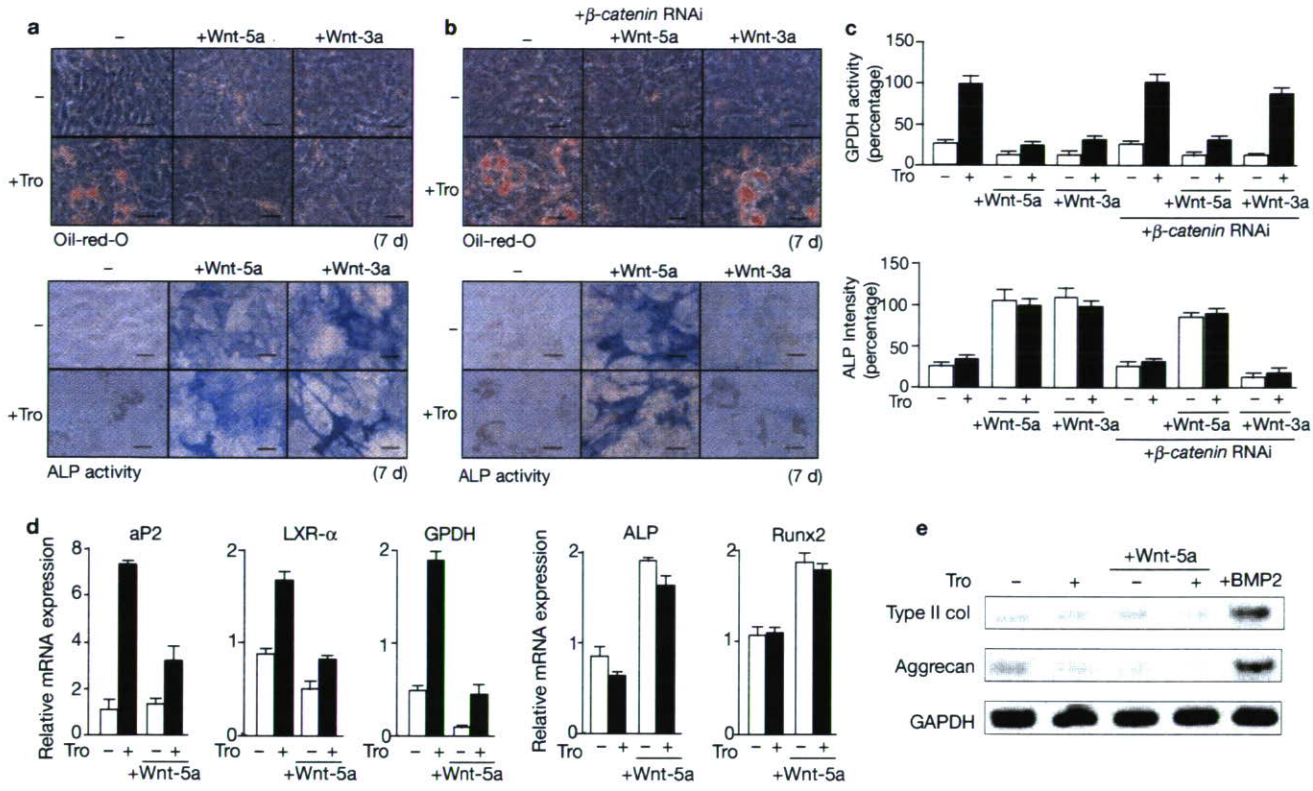


**Figure 2** Wnt-5a inhibits adipogenesis and induces osteoblastogenesis in bone marrow mesenchymal stem cells. (**a**) ST2 cells incubated with or without troglitazone (Tro), Wnt-3a or Wnt-5a for 7 days were stained with Oil-Red-O (top) or for alkaline phosphatase (ALP) activity (bottom). (**b**) After transfection with β-*catenin* RNAi, ST2 cells were incubated and stained as in **a**. (**c**) Top, glycerol-3-phosphate dehydrogenase (GPDH) activities were measured using a GPDH assay kit. Bottom, measurement graph of ALP activities ($A_{410}$) in each cell. Error bars represent the means±s.d. of triplicate determinations. $n=3\times10^6$ cells. (**d**) Quantitative RT–PCR of differentiation markers of adipocyte (aP2, GPDH, LXR-α) and osteoblast (Runx2 and ALP) in ST2 cells treated with/without Tro or Wnt-5a. Error bars represent the means±s.d. of triplicate determinations. $n=3\times10^6$ cells. Expression levels were normalized for GAPDH expression. (**e**) RT–PCR analysis for differentiation markers of chondrocyte (type II collagen and aggrecan) in ST2 cells incubated with or without Wnt-5a, BMP2 and Tro was performed. Scale bars, 100 μm.

co-repressors or co-repressor complexes that often contain histone deacetylases (HDAC), which render histones hypoacetylated. Ligand binding to NRs induces clearance of such HDAC co-repressors, leading to recruitment of a co-activator or co-activator complexes in which histone acetyltransferase (HAT) activity is often detectable[7,8]. Besides ligand-induced transactivation through co-regulator switching, NRs mediate ligand-dependent and -independent transrepression through cross-talk with other intracellular signalling pathways through multiple processes of gene regulation[9].

PPAR-γ is an important NR in many biological events such as cell differentiation and cell-lineage decisions[10–12]. In particular, adipogenesis from pleiotrophic mesenchymal stem cells is primarily induced by PPAR-γ upon agonist binding[13]. However, such PPAR-γ function in adipogenesis seems to be modulated through cross-talk with other cellular signalling pathways[14]. For instance, even though bone mesenchymal stem cells are primed by PPAR-γ agonists for adipogenesis, suppression of PPAR-γ function by cytokines in progenitor cells converts the cell fate of adipogenic precursors into osteoblastic cells[15]. Osteoblastogenesis is governed by a number of regulators including Wnt peptide ligands[16–18]. Canonical and non-canonical Wnt signalling pathways are activated by multiple Wnt ligands through binding to frizzled (Fzd) plasma-membrane receptors. During activation of the canonical pathway, stabilization and nuclear translocation of the intracellular transducer β-catenin induces it to associate with members of the TCF-LEF (T-cell factor lymphoid enhancer factor) family of transcriptional factors for transcriptional activation[19]. However, downstream cascades from the non-canonical signal[20,21] remain to be uncovered and their role in mesenchymal stem-cell differentiation remains obscure.

Osteoblastogenesis is dominant over adipogenesis in the bone marrow of young animals and the cell-differentiation balance between the two cell types is usually reversed in bone marrow of elder or osteoporotic animals[18]. Therefore, we reasoned that PPAR-γ function is suppressed in the bone marrow of young animals. In the present study, we reveal that transactivation of agonist-bound PPAR-γ is repressed by a non-canonical cascade activated by Wnt-5a through the phosphorylated H3-K9 HMKT, SETDB1 (refs 22, 23) in a complex with NLK (ref. 20) and CHD7 (chromodomain helicase DNA-binding protein 7; ref. 24). This leads to a change of cell fate from adipogenesis to osteoblastogenesis of bone marrow mesenchymal stem cells even in the presence of a PPAR-γ agonist. Thus, these findings reveal a new molecular mechanism where a signal from a cell membrane receptor leads to altered histone modification and changes in gene regulation and cell-lineage decisions.

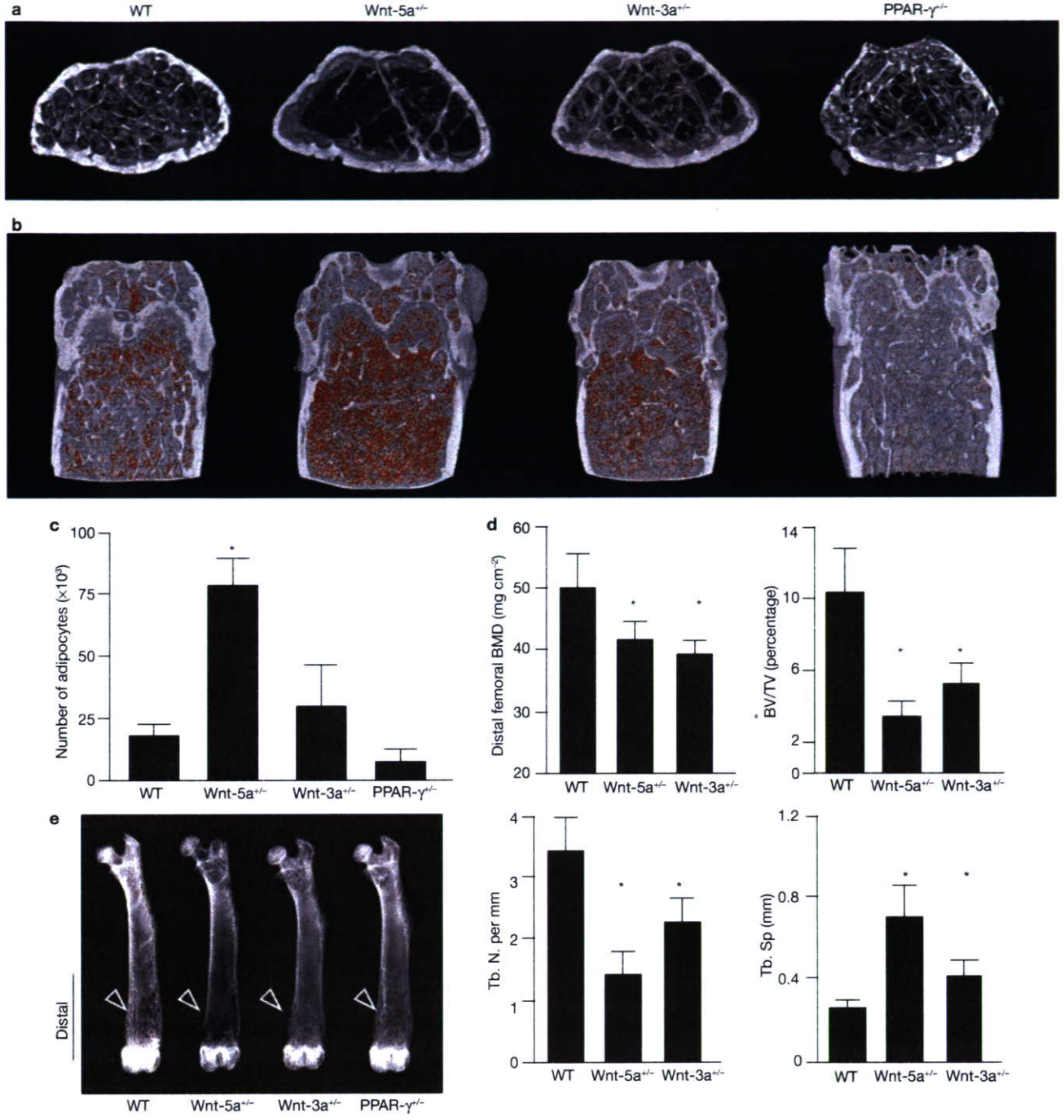


**Figure 3** Bone analysis of distal femora of 18-weeks-old WT, Wnt-5a$^{+/-}$, Wnt-3a$^{+/-}$ and PPAR-γ$^{+/-}$ male mice. (**a**, **b**) Three-dimensional computational tomography images of distal femora of representative WT, Wnt-5a$^{+/-}$, Wnt-3a$^{+/-}$ and PPAR-γ$^{+/-}$ mice. In (**b**), adipocytes are displayed as orange. (**c**) The number of adipocytes was histologically measured. (**d**) Bone mineral density (BMD) of distal femora, trabecular bone volume per tissue volume (BV/TV), trabecular number (Tb. N.) and trabecular space (Tb. Sp.) were measured on the CT image. In (**c**) and (**d**), bars indicate means±s.d.($n$=5 to 7 animals per genotype); Student's $t$-test; *, $P$<0.05 versus WT. (**e**) Soft x-ray image of femora from 18-week-old WT, Wnt-5a$^{+/-}$, Wnt-3a$^{+/-}$ and PPAR-γ$^{+/-}$ male mice.

## RESULTS

### NLK represses the transactivation function of PPAR-γ through a CaMKII–TAK1–TAB2 cascade

We previously reported that activated NF-κB transcriptionally represses activated PPAR-γ through a TAB1–TAK1-mediated (TAB1, TAK1-binding protein 1; TAK1, TGFβ-activated protein kinase 1) cascade activated by cytokines[15]. However, using TAB1$^{-/-}$ mouse embryonic fibroblast (MEF) cells[25], we unexpectedly found that TAK1 was still able to repress activated PPAR-γ in the presence of a synthetic agonist, troglitazone (Tro) (Fig. 1a). Because TAK1 serves as a mediator for other signalling cascades[20,26], we searched for a partner for TAK1 and found TAB2. By searching for downstream factors using a transient expression assay in ST2 cells (bone-marrow-derived stromal cells), a mitogen-activated protein (MAP)-kinase-like kinase, NLK, was found to replace TAK1–TAB2 and repress activated PPAR-γ (Fig. 1b). The wild-type (WT) and deletion mutants of NLK, which were potent repressors of PPAR-γ were

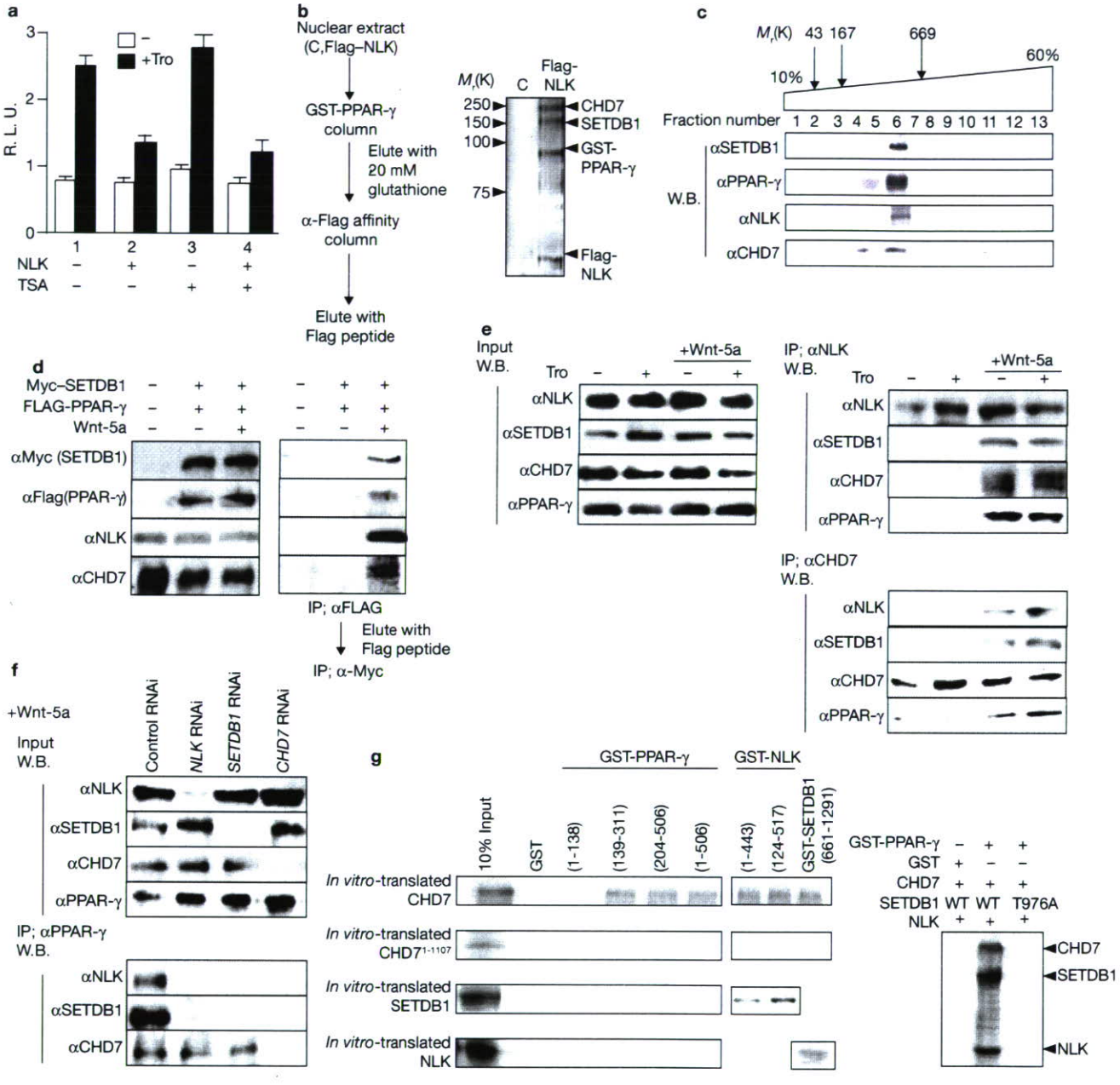


**Figure 4** SETDB1 and CHD7 form a complex with PPAR-γ and NLK in a Wnt-5a-dependent manner. (**a**) Luciferase assays in ST2 cells treated with or without HDAC inhibitor (1 μM TSA) after transfection with PPAR-γ and NLK expression vectors and PPRE-tk-luc vector. Error bars represent the mean±s.d. of triplicate determinations. (**b**) Purification of the PPAR-γ–NLK complex from Flag–NLK-expressing HeLa cells using GST–PPAR-γ affinity column followed by anti-Flag immunocolumn chromatography. (**c**) Analysis of NLK–PPAR-γ complex by glycerol density gradient followed by western blotting with anti-SETDB1 and anti-CHD7 antibodies. (**d**) Two-step immunoprecipitation. ST2 cells were transfected with Flag–PPAR-γ and Myc–SETDB1 and then treated with Tro and/or Wnt-5a. Nuclear extracts were immunoprecipitated with anti-Flag and eluted with the Flag peptide. Then anti-Flag immunocomplexes were immunoprecipitated with anti-Myc and probed by western blotting with indicated antibodies. (**e**) Immunoprecipitation assay in ST2 cells after treatment with or without Tro and Wnt-5a. Nuclear extracts were immunoprecipitated with anti-NLK and anti-CHD7 antibodies. Immunoprecipitants were detected by western blotting with indicated antibodies. Uncropped images of the blots are shown in the Supplementary Information, Fig. S6a. (**f**) Immunoprecipitation assay from cells RNAi-knockdown NLK, SETDB1 or CHD7. After infection with Adeno X-RNAi against NLK, SETDB1 and CHD7 in ST2 cells, cells treated with Wnt-5a were lysed and immunoprecipitated with anti-PPAR-γ antibody. Immunocomplexes were analysed by western blotting with indicated antibodies. (**g**) GST fusion proteins of NLK, PPAR-γ and SETDB1 were expressed in *E. coli* and used in GST pull-down assays with [$^{35}$S]-methionine-labelled CHD7 or CHD7$^{1-1107}$. Compared with CHD7, CHD7$^{1-1107}$ did not bind to PPAR-γ, NLK and SETDB1. When [$^{35}$S]-methionine-labelled CHD7, SETDB1 and NLK were incubated with GST-PPAR-γ, all components were associated with GST-PPAR-γ (right panel).

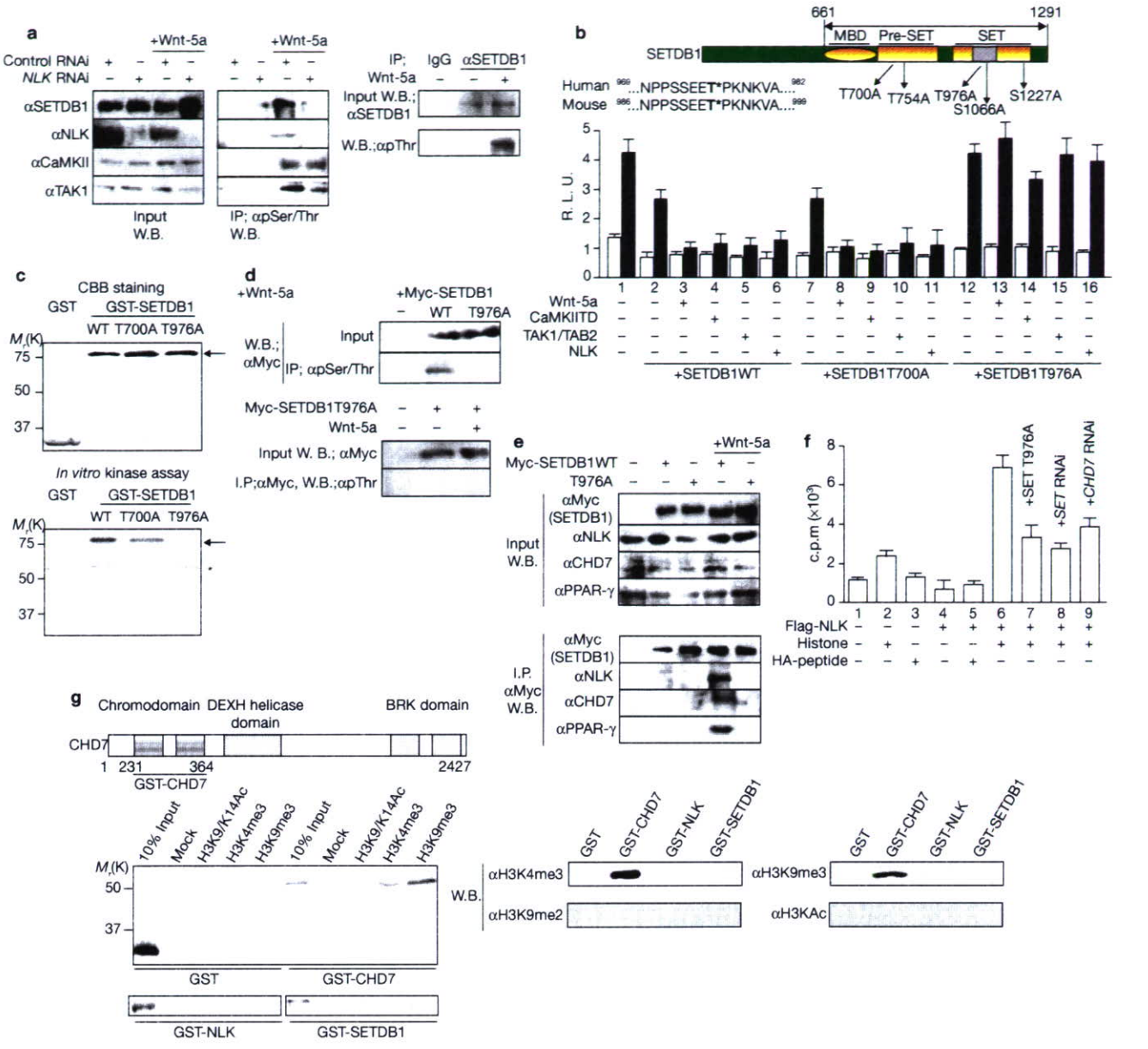


**Figure 5** Phosphorylated SETDB1 forms a complex with CHD7–NLK–PPAR-γ. (**a**) Left and middle panel, lysates of ST2 cells treated with or without Wnt-5a and transfected with control or *NLK* RNAi were applied to anti-Ser–Thr phosphorylation columns, then probed with indicated antibodies. Uncropped images of the blots are shown in the Supplementary Information, Fig. S6b. Right panel, lysates of ST2 cells treated with or without Wnt-5a were immunoprecipitated by IgG or anti-SETDB1 and then probed by anti-phosphothreonine (pThr). (**b**) Predicted phosphorylation sites of SETDB1 (661–1291). Thr976 is conserved between humans and mice. Luciferase assays in ST2 cells transfected with PPRE-tk-luc vector, PPAR-γ expression vector and indicated expression vectors were performed. Error bars represent the mean±s.d. of triplicate determinations. $n$=5×10⁴ cells. (**c**) NLK phosphorylates GST–SETDB1 *in vitro*. Upper panels, GST-fusion SETDB1 (WT, T976A and T700A) proteins were stained with CBB (upper panel, arrow indicates GST–SETDB1). Lower panels, the *in vitro* kinase assay was performed as described in the methods. (Arrow indicates GST–SETDB1, and the asterisk indicates self-phosphorylated NLK.) (**d**) SETDB1 T976A is not phosphorylated *in vivo*. Upper panel, after transfection with the indicated expression vector, immunoprecipitation with anti-Ser–Thr phosphorylation columns and western blotting was performed. Lower panel, after transfection with Myc–SETDB1T976A expression vector, cell extracts were immunoprecipitated with anti-Myc and probed with anti-phosphothreonine. (**e**) Immunoprecipitation assay in ST2 cells. After transfection with Myc–SETDB1 or SETDB1 T976A expression vector, immunoprecipitation with anti-Myc sepharose and western blotting were performed using the indicated antibodies. (**f**) NLK immunocomplexes possess histone methyltransferase activity. After transfection with Flag–NLK expression vector and the indicated vector and RNAi, in ST2 cells and immunoprecipitation with anti-Flag column, HMT assays were performed. Error bars represent the means±s.d. of triplicate determinations. $n$=5×10⁴ cells. (**g**) Upper panel, the peptide pull-down assay was performed using purified GST and GST-fused proteins with various modified H3 peptides (1–21 a.a.) indicated on top. Bound proteins were analysed by SDS-PAGE and silver staining. Lower panels, histone-binding assays were performed using HeLa histone extract and GST, GST–CHD7, –NLK and –SETDB1. Bound proteins were analysed by SDS-PAGE and western blotting. Uncropped images of the blots are shown in Supplementary Information, Fig. S6c.

localized in the nucleus (Fig. 1c, d). Although a kinase-negative mutant ($NLK^{K155M}$) was located in the nucleus (Fig. 1d), this mutant lost transrepressive activity for PPAR-γ (Fig. 1b).

CaMKII (calcium/calmodulin-dependent protein kinase II) is an upstream factor of TAK1–TAB2 that activates NLK for its repressive activity[20]. Treatment with KCl, which activates CaMKII, was effective in repressing PPAR-γ function (Fig. 1e). A constitutively kinase-dead form of CaMKII (CaMKII KD) and the CaMKII inhibitor KN93 abrogated the suppressive activity of NLK for PPAR-γ (Fig. 1e). Through investigating membrane-receptor ligand candidates that activate NLK in ST2 cells, we found that Wnt-5a mediated the suppressive function of NLK (Fig. 1f). However, Wnt-5a action was not abrogated by knockdown of β-catenin (Fig. 1f) and, unlike Wnt-3a, Wnt-5a did not activate the TCF-LEF-mediated canonical cascade (Fig. 1g).

### An activated non-canonical Wnt cascade attenuates adipogenesis through repression of PPAR-γ activity

Expression of Wnt ligands and their receptors was tested in ST2 cells. ST2 cells are derived from mouse bone marrow stromal cells and differentiate into either adipocytes through PPAR-γ activation or osteoblasts if induced by several cytokines[15]. We observed that Wnt-5a and several frizzled receptor genes are expressed at significant levels in ST2 cells as well as in mouse bone marrow cell primary culture (data not shown).

Wnt-5a, but not the canonical Wnt ligand Wnt-3a, was capable of repressing PPAR-γ function through NLK on synthetic (Fig. 1f) as well as natural PPAR-γ target gene promoters (see Supplementary Information, Fig. S1a). $TAK1^{K63W}$ (a kinase-dead mutant of MAPKKK), CaMKII KN as well as $NLK^{K155M}$ abrogated Wnt-5a-induced suppression of PPAR-γ (Fig. 1h). Furthermore, knockdown of NLK (see Supplementary Information, Fig. S2) abolished the effect of Wnt-5a, CaMKII and TAK1–TAB2 (Fig. 1b, e, f). Transactivation functions of adipogenic (CCAAT/enhancer binding protien (C/EBPβ), glucocorticoid (GR)) or osteoblastogenic (Runx2) transcriptional factors were not modulated by Wnt-5a treatment (Fig. 1i). It is notable that the activated non-canonical Wnt signalling by Wnt-5a lowered the basal activity of the tested PPAR-γ target gene promoters (see Fig. 1h for instance). Interestingly, PPAR-γ phosphorylation mutants (PPAR-γ S8A, S112A and S8A-S112A), which have been reported to be insensitive to MAPK (ERK)-induced suppression[14], remained susceptible to the suppressive action of NLK (see Supplementary Information, Fig. S1b).

Wnt-5a has been identified as a potential genetic determinant of diet-induced obesity[27] and so we examined the effect of Wnt-5a on ST2 cell differentiation. Treatment with Tro induced adipogenesis, lipid accumulation and glycerol-3-phosphate dehydrogenase (GPDH) activity (Fig. 2a, c) as reported previously[15,28]. Under these conditions, Wnt-5a seemed to mediate transdifferentiation of adipo-progenitors into osteoblastic cells expressing alkaline phosphatase (ALP) (Fig. 2a, c), as reflected by expression of markers of mature adipocytes (GPDH, aP2 and LXR-α) and osteoblasts (ALP and Runx2) (Fig. 2d and Supplementary Information, Fig. S1c), but not chondrocyte-specific markers (type II collagen and aggrecan) (Fig. 2e). Knockdown of β-catenin by RNA interference (RNAi) did not abrogate Wnt-5a-induced adipogenesis inhibition (Fig. 2b, c). Again, this supports the involvement of the non-canonical Wnt cascade activated by Wnt-5a in promoting osteoblastogenesis through attenuating adipogenesis with induction of Runx2, a critical osteoblastogenic transcription factor (Fig. 2d and Supplementary Information, Fig. S1c). Although TAZ (transcriptional co-activator with PDZ-binding motif) has recently been identified as an osteoblastogenic factor of mesenchymal stem-cell differentiation by repressing PPAR-γ function[29], TAZ seemed to be independent from the mechanism of Wnt-5a-induced suppression of the transactivation function of PPAR-γ (see Supplementary Information, Fig. S3a), and also independent from adipogenesis inhibition (see Supplementary Information, Fig. S3b). Together with the observation that *TAZ* gene expression is unaltered by Wnt-5a treatment (see Supplementary Information, Fig. S3c), we assume that the TAZ-mediated cascade does not converge with that of Wnt-5a in the differentiation of mesenchymal stem cells. Thus, activated PPAR-γ seems to potentiate cytodifferentiation of mesenchymal stem cells into adipo- or osteo-progenitors.

### Wnt-5a haploinsufficiency in mice induces bone loss with enhanced adipogenesis in bone marrow

As expected from the physiological effect of PPAR-γ on adipogenesis from mesenchymal stem cells in bone marrow[30], haploinsufficiency of PPAR-γ in mice ($PPAR\text{-}\gamma^{+/-}$) resulted in a reduction of adipocytes in bone marrow (Fig. 3b, c). Moreover, as expected from *in vitro* observations, bone mass increase, presumably because of increased osteoblastogenesis from bone marrow stem cells, was observed in $PPAR\text{-}\gamma^{+/-}$ male mice[31] (Fig. 3a, b, e). By contrast, $Wnt\text{-}3a^{+/-}$ males[32] exhibited bone loss (Fig. 3a, b, d, e), consistent with previous reports that canonical Wnt signalling is responsible for bone formation through stimulating osteoblastogenesis[33–35]. However, unlike $PPAR\text{-}\gamma^{+/-}$ mice, adipogenesis seemed unaffected in $Wnt\text{-}3a^{+/-}$ mice (Fig. 3b), suggesting that canonical Wnt signalling is unlikely to attenuate adipogenesis from adipo- or osteo-progenitor cells.

Supporting *in vitro* observations of Wnt-5a action, $Wnt\text{-}5a^{+/-}$ mice[36] showed a clear bone-loss phenotype, with decreased trabecular bone mass (Fig. 3d, and see arrow heads of Fig. 3e). Presumably, this was caused by reduced osteoblastogenesis as shown in the femur (Fig. 3a), which shows significantly elevated number of adipocytes in bone marrow (Fig. 3b, c) when compared with wild-type littermates. Taken together, these findings confirm that Wnt-5a potentiates the cell-lineage decision of bone marrow mesenchymal stem cells into osteoblasts, presumably through the non-canonical Wnt signalling pathway.

### NLK activated by Wnt-5a forms a complex with a HKMT

We then tested whether NLK-induced suppression of PPAR-γ function was linked to HDAC using the HDAC inhibitor, tricostatin A (TSA). However, TSA was unable to reverse NLK-mediated suppression of PPAR-γ function in ST2 cells (Fig. 4a). No alteration in PPAR-γ protein turnover was detected even when NLK was overexpressed (see Supplementary Information, Fig. S4a). Considering that NLK is a downstream factor of activated Wnt-5a (ref. 20), we reasoned that NLK might associate with unknown co-regulators to suppress PPAR-γ function. We therefore biochemically purified NLK-containing complexes from nuclear extracts of KCl-treated HeLa cells expressing Flag-tagged NLK by two-step purification[37,38] (Fig. 4b). We identified an NLK–nuclear-protein complex with a molecular weight of around 400–500 kDa by using glycerol gradient centrifugation fractionation (Fig. 4c). By MALDI-TOF mass spectrometric analysis of the other two complex components, two proteins (220 kDa and 170 kDa) were identified. The 220-kDa band was a DEXH-box and CHD-domain-containing ATPase protein, CHD7

(ref. 24). The 170-kDa band was an HKMT (SETDB1) that suppresses transcription through histone H3 methylation at K9 (refs 22, 23). We confirmed the formation of these complexes by a two-step immunoprecipitation assay (Fig. 4d) and association of endogenous NLK, SETDB1 and CHD7 in a complex with PPAR-γ was only detectable after treatment with Wnt-5a in ST2 cells (Fig. 4e). This Wnt-5a-induced association was abrogated when NLK, SETDB or CHD7 was knocked down by RNAi (Fig. 4f). In a GST pull-down assay, CHD7 seemed to be able to physically interact with NLK, SETDB1 and PPAR-γ, whereas PPAR-γ did not interact with SETDB1 (Fig. 4g). However, PPAR-γ seemed to associate with SETDB1 in the presence of CHD7 (Fig. 4g; lower panel).

### SETDB1 T976A phosphorylation by NLK is a prerequisite for HKMT activity and transrepression of PPAR-γ

We hypothesized that Wnt-5a-activated NLK phosphorylates SETDB1, because SETDB1 harbours several putative phosphorylation sites that could be NLK substrates (Fig. 5b). Using an anti-phosphorylated Ser–Thr antibody column, endogenous SETDB1 was found to be phosphorylated in a Wnt-5a-dependent manner (Fig. 5a). Wnt-5a-induced phosphorylation and repressive action on PPAR-γ was tested using SETDB1 deletion mutants (see Supplementary Information Fig. S4b). The mapped carboxy-terminal domain contains putative Thr–Ser phosphorylation site residues, and these were mutated to alanine (T700A, T754A, T976A, S1066A and S1277A; Fig. 5b). Among the five tested SETDB1 point mutants, only the T976A mutant was found to be deficient in SETDB1 repressive action (Fig. 5b) and was not phosphorylated by NLK either *in vivo* or *in vitro* (Fig. 5c, d). Interestingly, as a reflection of the importance of Thr976 phosphorylation for SETDB1 function, the region around Thr976 is highly conserved between human and mouse SETDB1 despite having only about 75% homology in adjacent regions (Fig. 5b). Significantly, Wnt-5a-induced complex formation of NLK–CHD7 with SETDB1 and PPAR-γ was abrogated by the T976A point mutation (Fig. 5e). The expected activity of the SETDB1 histone methyltransferase was detected in the NLK complex from Wnt-5a-treated ST2 cells (Fig. 5f). However, knockdown of either SETDB1 or CHD7 reduced the histone methyltransferase activity of the NLK complex (Fig. 5f), suggesting that SETDB1 requires assembly with NLK and CHD7 as a complex. Reflecting the presence of two chromodomains[39] in CHD7, CHD7 demonstrated physical interactions with tri-methylated H3-K4 and H3-K9 in a peptide pull-down assay and a histone-binding assay with semi-purified histones from HeLa cells (Fig. 5g). However, such preferential and significant interactions were not detected for acetylated H3.

### Wnt-5a-induced H3-K9 methylation represses PPAR-γ-dependent activation of PPAR-γ target gene promoters

We then performed a chromatin immunoprecipitation (ChIP) analysis of endogenous transcriptional factors and histone modifications at the PPAR-γ binding site (PPRE) of the aP2 gene promoter[13]. Tro treatment induced recruitment of known PPAR-γ co-activator SRC-1 and co-repressor N-CoR (Fig. 6a). Treatment with Wnt-5a for 6 h in the presence of Tro induced recruitment of NLK, CHD7 and SETDB1 to the proximal PPRE region, but not to the other distal region on the aP2 gene promoter. Furthermore, consistent with SETDB1 recruitment, an increase in histone di- and tri-methylation at histone H3-K9 was observed together with hypoacetylation of histone H3 (Fig. 6a). Similar findings were also observed with the other PPAR-γ target gene (LXR-α) promoter (see Supplementary Information, Fig. S5b). Such coordinated histone modification to inactivate chromatin was more evident when ST2 cells were treated with Wnt-5a for 7 d to induce osteoblastogenesis (Fig. 6b). In comparison, histone H3-K9 on the Runx2 promoter was highly acetylated, and recruitment of neither PPAR-γ nor SETDB1 was seen in the same cells treated with Wnt-5a (Fig. 6c). These observations suggested that the Runx2 gene promoter is transcriptionally active in the presence of Wnt-5a, consistent with induction of the *Runx2* gene during Wnt-5a-induced osteoblastogenesis (Fig. 2d and see Supplementary Information, Fig. S1c).

### Wnt-5-induced osteoblastogenesis from adipo- or osteoprogenitor cells requires NLK, SETDB1 and CHD7

With reference to these findings, we observed that overexpression of either NLK or SETDB1 was able to induce osteoblastogenesis rather than adipogenesis in ST2 cells (Fig. 7a, b; see Supplementary Information Fig. S2). Conversely, overexpression of an NLK mutant (NLK-KD) and SETDB1 mutants (SETDB1 T976A and ΔSET) and knockdown of NLK, SETDB1 or CHD7 induced adipogenesis rather than osteoblastogenesis even in the presence of Wnt-5a (Fig. 7a–d). Furthermore, these knockdowns abrogated the Wnt-5a-induced H3-K9 methylation and subsequent histone modification in the aP2 gene promoter (compare Fig. 6b with 7e).

## DISCUSSION

Activated PPAR-γ is remarkably potent in cytodifferentiation, and several co-regulators of PPAR-γ, and cross-regulation by other cellular signalling pathways, have been previously described[10–12]. In particular, during PPAR-γ agonist-induced adipogenesis from bone marrow mesenchymal stem cells, activated PPAR-γ seems to function at multiple steps of the cytodifferentiation process. This is evident because bone marrow mesenchymal stem cells are pleiotropic and can differentiate into osteoblasts, chondrocytes or myoblasts depending on the activities of cell-lineage determinants[17].

In this study, we have found that Wnt-5a induces osteoblastogenesis through attenuating PPAR-γ-induced adipogenesis in mesenchymal stem cells of bone marrow. Wnt-5a activated a non-canonical Wnt signalling cascade mediated through CaMKII–TAK1–TAB2–NLK, but did not trigger the β-catenin–TCF canonical Wnt signalling pathway. Wnt signalling pathways have previously been described as being able to cross-talk with signalling pathways of certain NRs[40,41], and the pivotal roles of such cross-talk in cell-fate decisions have recently been verified in *Caenorhabditis elegans*[42]. This would suggest that such cross-regulation is conserved in metazoans. However, unlike the non-canonical Wnt cascade presented here, the canonical pathway mediated through β-catenin–TCF is known to co-activate the transactivation function of activated NRs including PPAR-γ (refs 40, 41). Thus, it is likely that Wnt ligands, in a positive or negative manner, modulate the functions of NRs in transcriptional control, depending on their specific downstream signalling cascades.

Osteoblastogenesis was induced by Wnt-5a in ST2 cells even in the presence of a PPAR-γ agonist. Supporting these *in vitro* observations, Wnt-5a$^{+/-}$ mice exhibited a reduction in bone mass presumably because of a reduced number of osteoblasts whereas increased numbers of adipocytes were seen in the bone marrow (Fig. 3b). Bone mass decrease was also detectable in Wnt-3a$^{+/-}$ mice (Fig. 3a, b, d, e) presumably owing to

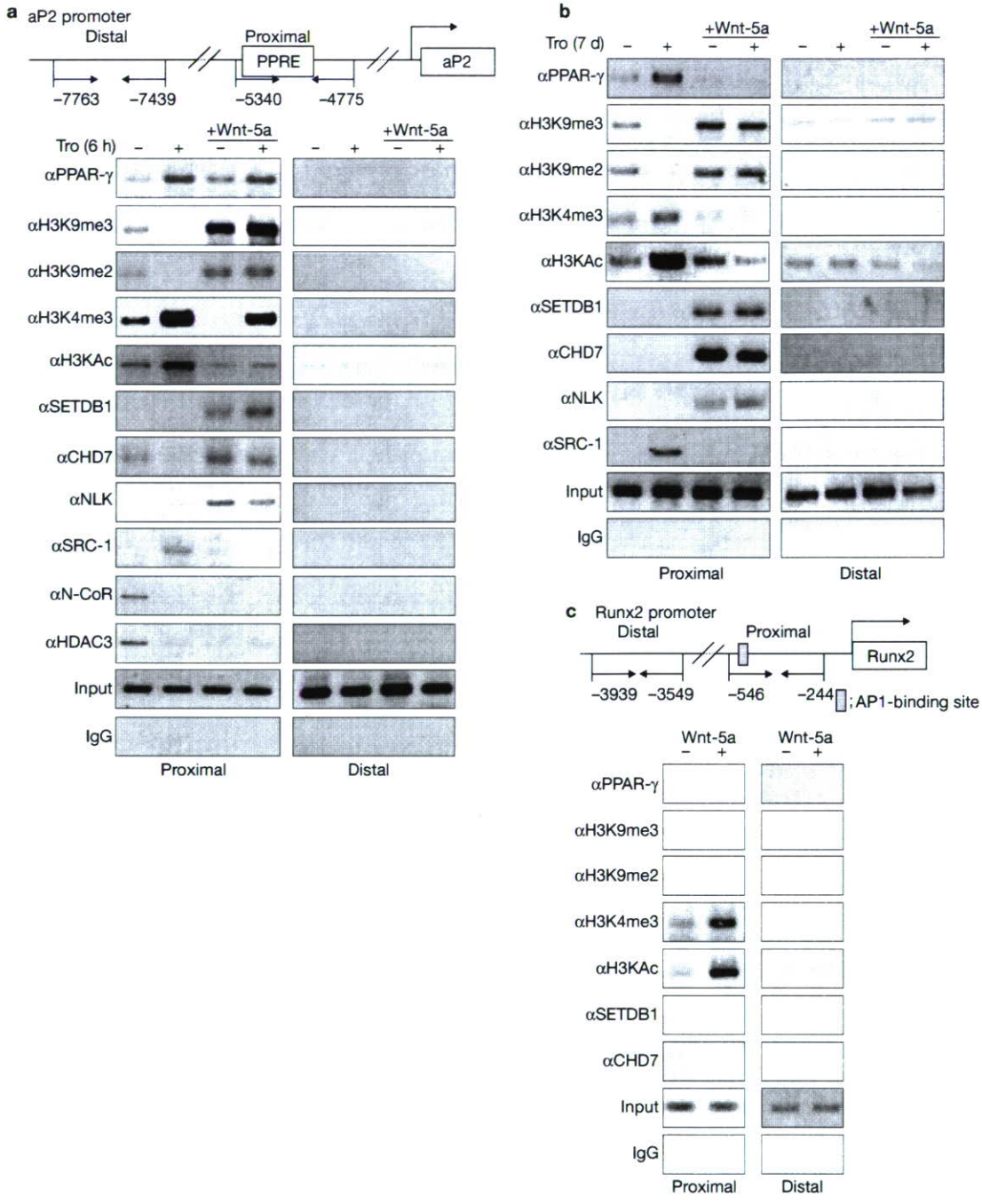


**Figure 6** Wnt-5a-dependent recruitment of NLK containing corepressor complex. (**a**, **b**) Chromatin immunoprecipitation analysis of the aP2 promoter in ST2 cells treated with or without Troglitazone and Wnt-5a for 6 h (**a**) or 7days (**b**) was performed using indicated antibodies. (**c**) ChIP analysis of Runx2 promoter in ST2 cells. ST2 cells were treated with or without Wnt-5a, and ChIP analysis was performed using indicated antibodies.

impaired canonical Wnt signalling, consistent with recent reports that the canonical Wnt cascade through LRP5–β-catenin (LRP5: low-density lipoprotein receptor-related protein 5) is indispensable for osteoblastogenesis[33–35]. Wnt signalling thus seems to contribute to osteoblastogenesis from bone marrow mesenchymal cells through both canonical and non-canonical cascades. However, in terms of preventing the adipogenesis cell-lineage decision, only non-canonical Wnt signalling plays a significant part in bone marrow development.

It was recently reported that TAB2 in macrophage cells activated by the IL-1 signalling cascade prevents clearance of an HDAC co-repressor complex from ligand-bound sex steroid receptors, thus maintaining a transcriptionally repressive state of the steroid receptor[43]. In the present study, interestingly, an HDAC inhibitor (TSA) failed to abrogate the Wnt-5a effect on PPAR-γ transrepression (Fig. 4a), and, consistent with this finding, HDAC3 and N-CoR were not detected 6 h after Wnt-5a treatment (Fig. 6a). However, before Wnt-5a treatment in the absence of Tro, HDAC3 and N-CoR were associated with the promoter (Fig. 6a and Supplementary Information, Fig. S5a), and Wnt-5a seemed to induce clearance of the N-CoR-HDAC complex and block SRC-1 recruitment even in the presence of Tro. These findings clearly suggest that the